ISUAAAT16-57

IMPROVEMENT OF THE "TRIPLE-PLANE PRESSURE MODE MATCHING TECHNIQUE" AND APPLICATION TO HARMONIC BALANCE SIMULATIONS

Sébastien Guérin

Institute of Propulsion Technology, German Aerospace Centre (DLR),
Department of Engine Acoustics, Berlin, Germany

ABSTRACT

The "triple-plane pressure mode matching technique" developed by Ovenden and Rienstra to analyse the acoustic field generated by turbomachine components is applied to Harmonic Balance calculations. Three extensions of the original method are assessed. They aim at improving the results with respect to i) the presence of swirl, ii) radial mean flow variations, and iii) the need to filter out convective pressure fluctuations. The method is applied to three generic test cases and two realistic examples: a low-speed fan stage and a high-pressure turbine exhibiting a strong swirl in the intra-stage. The extension to include radial variations of the mean flow in the calculation of the eigenmodes considerably improves the accuracy of the results, most notably for acoustic fields with a sparse modal content. At high Mach number, the accuracy of the simplistic analytical solution for a solid body swirl performs reasonably well because the large error made on each mode is statistically counterbalanced by the large number of contributing modes. The extension that includes an additional basis of convective pseudo-modes contributes to improve the results behind a cascade of blades, where wake perturbations are strong.

Keywords: acoustic level, modal decomposition, URANS and NLH method

NOMENCLATURE

A_n	pressure amplitude (Pa)
BPF	blade passing frequency
c	speed of sound (m·s^{-1})
c_p	constant-pressure specific heat (J·kg^{-1}·K^{-1})
C_{mn}	modal convection factor
$\mathcal{F}_n$	radial shape function (-)
k	wavenumber (m^{-1})
I	acoustic intensity (W·m^{-2})
$k_n^{\pm}$	acoustic axial wavenumber (m^{-1})
m, n	circumferential, radial mode order
P, p	mean, unsteady pressure (Pa)
PWL	sound power level (ref. 10^{-12} W)
R	radius at tip (m)

R_{univ}	specific gas constant (287.05 J·kg^{-1}·K^{-1})
U, u	mean, unsteady velocity (m·s^{-1})
η	hub-to-tip ratio (-)
Π	acoustic power amplitude (W)
ρ	mean density (kg·m^{-3})
γ	specific heat ratio (-)
ω	angular frequency (rad·s^{-1})
Ω	angular speed (rad·s^{-1})
x, r, θ	axial, radial, azimuthal component
HB	Harmonic Balance
RMA	Radial Mode Analysis using Bessel modes
TPP	Triple-Plane Pressure mode matching tech.
XMA	eXtended RMA (numerically calc. modes)
XTPP	TPP extended to convected perturbations
eq	equivalent value
rot	rotating frame
$\pm$	down-/upstream direction
$*$	complex conjugate

1. INTRODUCTION

Harmonic Balance (HB) [1] is used at DLR to predict the tonal acoustic field created by turbomachine components, like fans and turbines. The accurate prediction of acoustic levels requires two conditions: 1) the HB simulation is carefully carried out and 2) the acoustic field can be properly extracted and quantified.

Fulfilling the first condition requires that the models implemented in the solver have been verified and their application validated. The use of a solver also implies the definition of guidelines regarding the numerical setup and the meshing strategy, which are acquired at the price of extensive validation. Once the calculation has been performed, extracting the acoustic field (step 2) is useful for two reasons: i) the direct exploitation of the results and ii) their utilisation to verify that the simulation was correctly set up. This second reason is no less important since it validates or not the exploitation of the simulation. Thus, an accurate quantification of the acoustic levels at several positions of the computational domain can allow a precise analysis of the numerical dissipation [2], the reflections

at the domain boundaries, and the convergence of the simulation [3]. Once the simulation is validated, extracting the acoustic levels can be used to for instance compare different blade designs [4], determine radiation coefficients at duct extremities [5], assess the acoustic transmission through a rotor [2], etc.

The extraction of the acoustic field from turbomachine flow simulations requires to isolate the acoustic component from the other unsteady perturbations (vorticity and entropy) and characterise the acoustic field in terms of amplitude and direction of propagation. The method chosen by DLR is based on the triple-plane pressure mode matching technique (acronym TPP) developed by Ovenden and Rienstra [6]. This method works with unsteady pressure, which is by nature a good tracer of acoustic disturbances and conversely a weak marker of vorticity. Some other methods utilise the velocity, too. Refer to Giacché et al. [7] for a comparison of the two approaches. In TPP, a least-square fit is performed between the CFD data extracted at several–at least three–axial positions and a set of acoustic eigenmodes. The basis of eigenmodes chosen in the original formulation of TPP is valid for uniform flow, which is a crude approximation for real flows solved by means of the Navier-Stokes equations. When the conditions assumed to calculate the eigenmodes differ too much from those of the simulation because the mean flow is complex or the unsteady pressure field is dominated by convected pressure fluctuations, like e.g. in the blade wakes near the trailing edge behind a stator cascade, the fitting does not optimally work. The resulting error can alter the quality of the results.

In this work, two different options to better consider the complexity of the background mean flow in the calculation of the eigenmodes are considered. The first solution is still analytical. It aims at accounting for the presence of a solid body swirl. It is based on the analytical solution for uniform axial flow, modified as proposed by Morfey [8]. This extension is strictly valid for flows with a rigid body swirl ($U_\theta = \Omega r$) at low Mach number. The second option is classified as "numerical" since it solves radially-discretised perturbation equations. The solution extends the complexity to sheared, swirling mean flows and therefore, is more general.

In this paper, the extensions of the TPP method are briefly introduced. This includes a description of the method chosen to calculate the equivalent solid body swirl used together with the Bessel's analytical eigenmodes, an introduction to the extended TPP method, which uses an extra basis for convective modes, and the presentation and validation of the more elaborate approach that accounts for the radial flow profiles. Next, the extensions are applied to some generic test cases as well as to two simulations of HB configurations, representative of a low speed fan and a high-pressure turbine respectively. Based on the comparison of the results, the extensions are discussed.

2. METHODS
2.1 Equivalent mean flow
The mean flow saved on the three extraction planes has to be processed before it can be used to determine the acoustic eigenmodes. At first, a simple area averaging is performed to the flow in the azimuthal direction. Furthermore, the radial

velocity is discarded. (This is compatible with the slowly varying duct assumption.) For the approach that can account for the radial mean flow variations, the one-dimensional pressure profile is further corrected to satisfy the radial equilibrium. The simplistic analytical approach requires additional processing to somehow match the radial mean flow profiles to the rigid body swirl hypothesis. The chosen method assumes an equivalent flow with the same:

- net force:

$$F = 2\pi \int_{\eta R}^{R} Pr dr = P_{eq}\pi R^2(1 - \eta^2) \qquad (1)$$

- mass flow:

$$\dot{m} = 2\pi \int_{\eta R}^{R} \rho U_x r dr = \rho_{eq}U_{x,eq}\pi R^2(1 - \eta^2) \qquad (2)$$

- angular momentum:

$$M_\theta = 2\pi \int_{\eta R}^{R} \rho r^2 U_\theta dr = \frac{1}{2}\rho_{eq}\Omega_{eq}\pi R^4(1 - \eta^4) \qquad (3)$$

- enthalpy flow:

$$F_h = 2\pi \int_{\eta R}^{R} \rho c_p T U_x r dr = \dot{m} c_p T_{eq} \qquad (4)$$

The axial velocity $U_{x,eq}$ is given by

$$U_{x,eq} = \frac{R_{univ}}{c_p}\frac{F_h}{\pi R^2(1 - \eta^2)P_{eq}} = \frac{\gamma - 1}{\gamma}\frac{F_h}{F}. \qquad (5)$$

There are different thinkable options to determine the representative average values of a mean flow. The best averaging technique may depend on the target quantity as discussed by Cumpsty and Horlock [11]. The method presented here corresponds to the best option found among several. It does not include any acoustic criterium, however. In the asymptotic limit of a weak swirl, this averaging technique returns the correct angular speed for a solid body swirl.

2.2 Extensions of TPP
The method used at DLR Berlin is based on the approach proposed by Ovenden and Rienstra [6]. The principle is to match the unsteady pressure field extracted from–at least three–planes at constant axial positions with a set of acoustic eigenmodes. The pressure amplitude of the acoustic modes is obtained by minimising the difference between the simulation data and the model. This is repeated for each frequency ω and each azimuthal component m separately. As the duct cross-section of turbomachines often vary along the axis–while remaining axisymmetric, the TPP method uses the multi-scale approach to approximate the impact on the acoustic field. In the context of acoustic modes in ducted flow, the multi-scale approach is valid for slowly varying ducts and for modes far from the cut-on limits.

Compared to the original TPP formulation, the DLR method contains two extensions: 1) A new basis of pseudo-modes is introduced to better discard the convective perturbations as proposed by Weckmüller, Wohlbrandt and Guérin [12][13]. 2) Instead of the Bessel modes, acoustic eigenmodes considering radial mean flow variations can be calculated by using a normal mode analysis as proposed by Kousen [14] and applied.

For simplicity, only the case with axially-constant duct contours is treated below. The model assumes that the complex unsteady pressure $\hat{p}$–reduced to a single circumferential mode by Fourier transforms[1]–can be decomposed as follows,

$$\hat{p}(x,r) \approx \sum_{n=0}^{\infty} A_n^{\pm}(x_{ref}) \mathcal{F}_n^{\pm}(r) e^{ik_n^{\pm}(x-x_{ref})} \qquad (6)$$
$$+ A_n^c(x_{ref}) \mathcal{F}_n^+(r) e^{ik_c(x-x_{ref})},$$

where the superscript $\pm$ indicates the direction ("+" for the downstream, "−" for upstream), A_n denotes the complex pressure amplitude of the modes at radial order n for a reference axial position x_{ref}, $\mathcal{F}_n$ the radial shape of the acoustic eigenmode, k_n the acoustic axial wavenumber and k_c a convective wavenumber defined as

$$k_c = \frac{\omega}{U_x} - \frac{m}{r}\frac{U_\theta}{U_x}. \qquad (7)$$

The modal amplitude A_n is found by solving a least mean square problem following the method proposed in [6]. Notice that:

- In the analytical solution, the radial eigenfunction $\mathcal{F}_n$ is equal in both directions $(+)$ and $(-)$.
- Compared to [13], the convective wavenumber definition in Eq. (7) has been appended with the second term to account for the effect of swirl.
- The amplitude of the convective modes A_n^c cannot be physically interpreted. However, they can be used to reconstruct the vorticity perturbation as showed in [13].

Vilenski and Rienstra [15][16] proposed to include the convective eigenmodes of the linearised Euler equations to improve the mode matching. However, they pointed out the drawback of such an approach in reason of the difficulty to determine the set of convective eigensolutions.

The acoustic power Π is calculated using the formula provided by Morfey [17], which is strictly valid for irrotational homentropic flow:

$$\Pi = \left| \int_0^{2\pi} \int_{\eta R}^R I_x r \, dr \, d\theta \right|, \qquad (8)$$

where the acoustic axial intensity I_x is given by

$$I_x = \frac{1}{2} \Re \left\{ (1 + M_x^2)\hat{p}^* \hat{u}_x + \frac{M_x}{\rho c}\hat{p}^* \hat{p} + \rho c M_x \hat{u}_x^* \hat{u}_x \right.$$
$$\left. + M_x M_\theta \hat{p}^* u_\theta + \rho c M_\theta \hat{u}_x^* \hat{u}_\theta \right\}. \qquad (9)$$

The variables ρ, c, and M refer to the local value of mean flow and u to the acoustic particle velocity. The power amplitude is calculated by using the equations presented in Appendix.

2.3 Basis of eigenmodes

The propagation of acoustic waves in pipe flows has been the focus of many theoretical studies. The following discussion is restricted to straight annular ducts of constant circular cross-section.

First let us consider the case of a homogeneous mean flow. The following exponential description $\phi(x,r,\theta,t) = \phi(r)e^{i(k_x x + m\theta - \omega t)}$ is applied to the acoustic disturbance, where the acoustic field has been assumed to be time-periodic of angular frequency $\omega \in \mathbb{R}$ and 2π-periodic in circumference with $m \in \mathbb{Z}$ the corresponding mode order, and to have an axial wavenumber $k_x \in \mathbb{C}$. With this assumption it becomes possible to describe the radial variation of the perturbed pressure $p(r)$ by a single second order ordinary differential equation (ODE), for which there exists a discrete set of acoustic eigenmodes. For an annular duct the solution $p(r)$ is obtained by a combination of mth-order Bessel and Neumann functions [18]. The radial wavenumber depends on the impedance boundary conditions at the wall [19]. The axial wavenumber k_x is related to the radial wavenumber and the free-field wavenumber $k = \omega/c$ by the acoustic dispersion relation. If k_x is purely real then the signal amplitude is periodic in axial direction. If k_x contains an imaginary part, the pressure signal decays exponentially along the duct axis: the mode is said to be cut-off or evanescent.

The sound field transmission in axially constant shear flows–i.e. with a radial variation of the axial speed and no pressure gradient–is governed by a single second order partial differential equation on the perturbed pressure, sometimes called Pridmore-Brown equation in reference to the author [20]. For cylindrical axial shear flows, using the aforementioned exponential assumption, the pressure equation reduces to a single ODE, which can be solved numerically [21]. There is no analytical solution in the general case.

Axially constant swirling flows are substantially more complex to characterize [22][23][24][25][26][27]. An eigenmode analysis yields a discrete family of pressure-dominated nearly-sonic modes. It may also contain a discrete set of velocity-dominated nearly-convected modes, instabilities and a continuum of modes with critical layers. Here also an ODE can be found for $p(r)$, the solution of which can be retrieved after integration. An alternative approach using the normal mode analysis directly applied to the linearised Euler equation was proposed by Kerrebrock [28] and Kousen [14]. A system of radially-discretised linearised perturbation equations is formulated as a generalised eigenvalue problem. Notice the work done by Golubev and Atassi [22], who considered a potential swirling flow. They use this property that any incident acoustic field propagating in the flow does not create unsteady vortices.

The TPP method as originally published by Ovenden and Rienstra [6] relies on the analytical solution to determine the acoustic eigenvalues k_n and the eigenvectors $\mathcal{F}_n$. The eigensolutions are retrieved from the wave equation for a

---

[1] Unless it is necessary for clarity, like e.g. in Eq. (10) to (12), the azimuthal order m is not indicated in the equations in order to simplify the notations.

uniform mean flow with hard walls. When a rigid body swirl is added within the limit of small Mach number, that is $M_\theta \ll 1$, the radial eigenfunction remains identical but the axial wavenumbers and the cutoff limits are modified. The description of the acoustic modal solution in vortical mean flows proposed by Morfey [8] is used as model in the present TPP implementation. Thus, the axial wavenumber is given by

$$k_{mn}^\pm = \frac{k\delta_m}{1-M_x^2}(-M_x \pm \alpha_{mn}), \qquad (10)$$

and the cut-on factor α_{mn} by

$$\alpha_{mn} = \sqrt{1 - \frac{(1-M_x^2)}{\delta_m^2}\frac{\sigma_{mn}^2}{(kR)^2}}. \qquad (11)$$

The swirl factor δ_m defined in Eq. (12) introduces a dissymmetry between co- and contra-rotating modes. The swirl in the flow increases the tendency of an acoustic mode to become cut-off if the swirl Mach number and the circumferential mode have the same rotational direction, as also showed by Roger and Arbey for simplified solid body swirl and free vortex flows[29].

$$\delta_m = 1 - \frac{mM_{\theta,tip}}{kR} \qquad (12)$$

If the tendency given by Eq. (10) to (12) are correct, the analytical solution lacks of accuracy for real flows. The discrepancy increases with the Mach number. In order to circumvent this problem and reduce the inaccuracy, a method able to account for the radial flow profiles was implemented. The chosen approach relies on the normal mode analysis applied to the isentropic linearised Euler equations as proposed by Kousen [14]. Hard-wall boundary conditions are imposed at the hub and casing. A system of radially-discretised perturbation equations is formulated as a generalised eigenvalue problem, the solution of which is solved by using the QZ-algorithm. A Chebyshev grid–which advantageously uses a higher density of points in the boundary layer–is used for the spatial discretisation and the spectral derivative matrix is calculated accordingly. The method provides $4 \times N_r$ solutions, where N_r is the number of collocation points. A sorting algorithm was developed to sort out all but the acoustic modes[2]. Acoustical modes badly resolved are also discarded. The sorting is based on the wavenumber spectrum and the pressure eigenvectors. At first the full space of solutions is reduced to a domain of interest. Then solutions such as $p/\rho c u_x < 0.1$ are discarded. This ratio is typically high for sonic modes and low for convective modes. The solutions are then split in cut-on ($\Im(k_n) = 0$) and cut-off modes ($\Im(k_n) \neq 0$). The cut-on modes are sorted between downstream and upstream propagating waves. For that, a small imaginary part ($1E{-}5 \times k$) was added to the frequency when the matrix had been built. If $\Im(k_n) > 0$ (resp. $\Im(k_n) < 0$), the cut-on acoustic mode propagates in the upstream (resp. downstream) direction. This very efficient technique was proposed by Moinier and Giles [10].

---

[2] One of the advantages of Bessel solution is that it does not require a sorting algorithm and the solution is more robust.

TC	Ref	Type of flow	$k_{tip}R$	m
PF1b		Uniform axial flow with $M_x = 0.477$ ($M_\theta = 0$)	9.82	0
SH3	[30]	Shear flow with $0.3 < M_x < 0.6$ ($M_\theta = 0$)	15	3
SH4a	[30]	Boundary layer profile with $\max(M_x) > 0.5$ ($M_\theta = 0$)	15	13
SW2	[14] [25]	Free vortex flow with $M_x = 0.5$ and $\max(M_\theta) > 0.5$	10	2
SW3	[31]	Rigid body + free vortex mean flow with $M_x = 0.5$ and $\max(M_\theta) > 0.2$	25	15
RS1	[31]	RANS profiles with $\max(M_x) > 0.3$ and $\max(M_\theta) > 0.3$	22	7

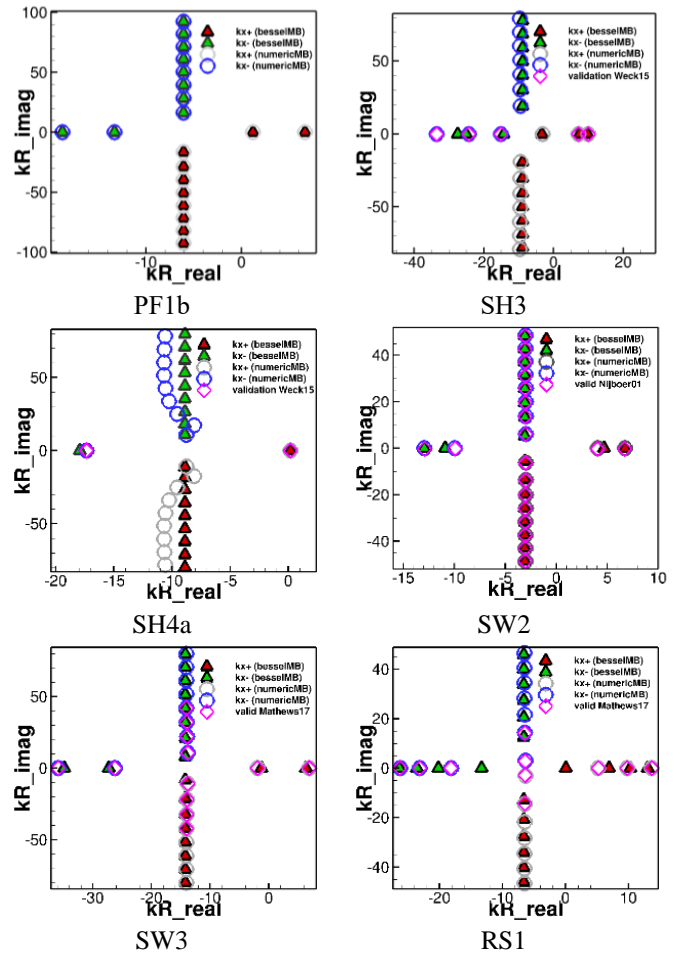TABLE 1: VALIDATION TEST CASES FOR THE EIGENSOLUTIONS OF SHEARED SWIRLING FLOWS

FIGURE 1: FOR THE TEST CASES OF TABLE 1, COMPARISON BETWEEN THE EIGENVALUES k_n OBTAINED ANALYTICALLY (Δ), NUMERICALLY (O) AND THE VALIDATION DATA (◊)

The implementation of the method has been verified and validated. The first validation for the shear flow formulation was

showed by Weckmüller et al. [30]. Since then, the formulation has been extended to swirl. Some of the validation cases used in the current development suite are presented in Table 1. With the exception of PF1b, which compares the numerical solution with the Bessel solution for a plug flow, the test cases were found in the literature. For the sake of conciseness, the flow profiles are not shown but can be found in the cited publications. All the test cases assume an homentropic flow. The comparison of the radial eigenfunctions is skipped too and only the comparison of the wavenumber spectrum is shown in Figure 1. While there are some noticeable differences between the Bessel solutions and the validation data, there is an excellent agreement between the numerically calculated solution and the validation data.

3. RESULTS AND DISCUSSION

The objective of Section 3 is to apply the different formulations of the method described above to some well-controlled simulations and two more realistic configurations. In the following, the label RMA (resp. XMA) denotes the solution calculated by using the analytically (resp. numerically) calculated set of eigenmodes.

3.1 Generic test cases

The generic test cases were designed with the objective to have only a single acoustic mode present in the computed solution. The Euler equations were applied. The duct contours are constant and the flow is axially constant. Note that the TPP approach (without the convective pseudo-modes) is applied since the simulations are supposed to be (nearly) free from vorticity.

The first test case is a validation test case, which corresponds to the same plug flow as used for PF1b presented in Table 1. The simulation result is showed in Figure 2 for the real part of the pressure. The mean flow profile is imposed at the inlet, which is located on the left-hand side of the figure. An upstream-propagating wave with $(m, n) = (3,1)$ is prescribed at the outlet of the computational domain (on the right-hand side of the figure). Phase-shifted boundary conditions are imposed in the HB simulation, therefore, only one duct segment is simulated. The full annular disk on the figure represents the pressure saved onto the three planes used to perform the mode analysis. The constant profiles in solid lines shown on the right-hand side diagrams correspond to the mean flow of the simulation.

The results of the mode analysis of RMA and XMA are in excellent agreement down to the last detail as seen in Figure 3. This indicates that the used 2D gust and the non-reflecting boundary conditions are well performing in this case. It should also be noticed that the three different methods to determine the power amplitudes give the same results as Table 2 shows.

Method	PWL+ (dB)	PWL- (dB)	ΔPWL (dB)
RMA	26.60	83.23	56.60
XMA	26.61	83.23	56.60
direct integration	PWL = 83.24 dB		-

TABLE 2: SOUND POWER LEVEL FOR SIMULATION PF1
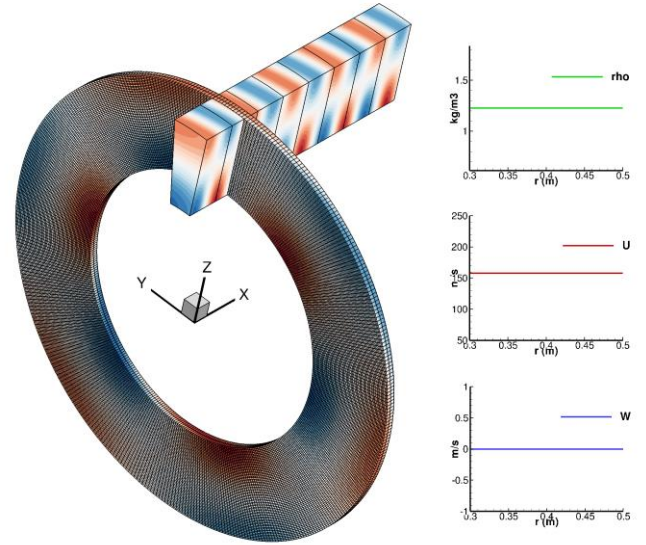

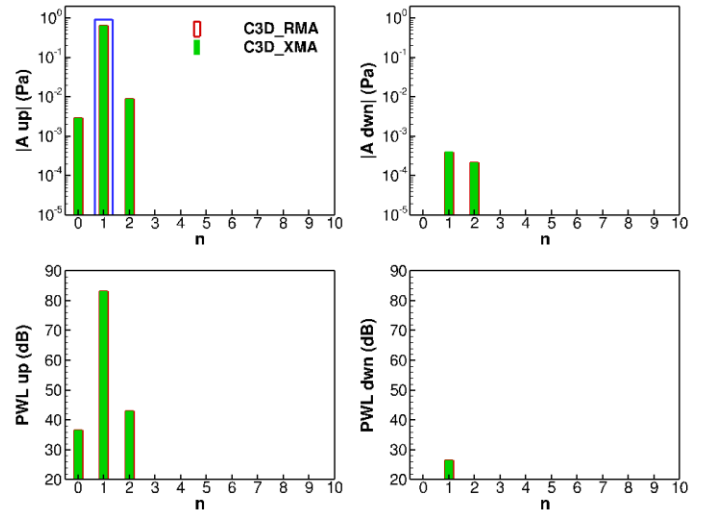**FIGURE 2:** GENERIC TEST CASE PF1 WITH PLUG FLOW

FIGURE 3: ACOUSTIC MODE ANALYSIS OF SIMULATION PF1; THE TARGETED MODE IS INDICATED IN BLUE

The second test case corresponds to the test case SH3 of Table 1. Now, there is a strong shear profile with an inflection point located at about 2/3 of the span. The equivalent mean flow calculated using Eq. (1) to (5) and used by RMA is indicated by the dashed lines. The same acoustic mode $(m, n) = (3,1)$ as before is targeted using the numerically calculated eigensolution. The simulation does not indicate any strongly visible radial mode scattering and the acoustic pattern remains well repetitive along the axis. This suggests that the used 2D gust and the non-reflecting boundary conditions are rather well performing in this case too.
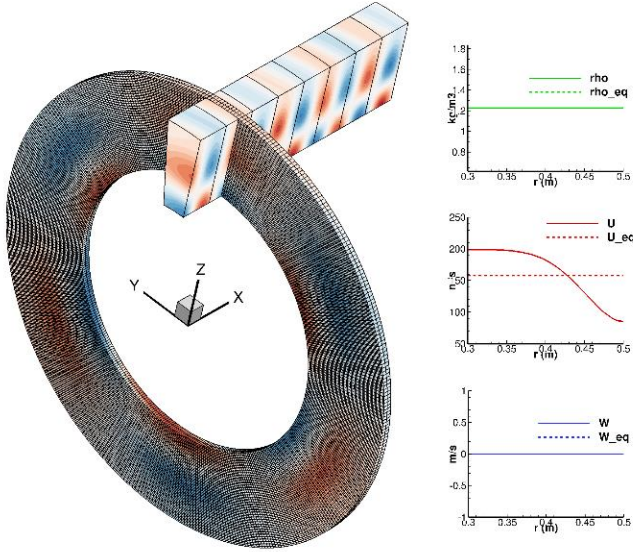
FIGURE 4: GENERIC TEST CASE SH3 WITH SHEAR FLOW

The results of the mode analysis are presented in Figure 5. The amplitudes obtained with XMA reveals that the targeted mode is dominant by about one order of magnitude compared to the next strongest mode and by about two orders of magnitude compared to its reflections. The RMA approach completely fails. If it should be used, the interpretation of the results would be erroneous. Even in terms of total sound power (see Table 3), the results provided by RMA are not satisfactory. Indeed, the XMA results indicate a sound power difference of 46.61 dB between the up- and downstream propagating modes, while the RMA method leads to only 5.50 dB difference. In terms of total sound power, the agreement between the direct integration with Eq. (8) and (9) and the XMA results (Eq. (17)) is excellent even though the flow is rotational and the cross-terms, due to the fact that the modes are not orthogonal, are neglected.
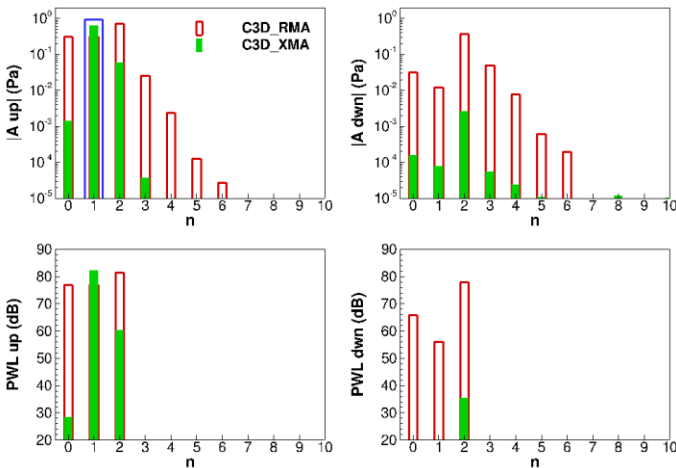
FIGURE 5: ACOUSTIC MODE ANALYSIS OF SIMULATION SH3; THE TARGETED MODE IS INDICATED IN BLUE

Method	PWL+ (dB)	PWL- (dB)	ΔPWL (dB)
RMA	78.20	83.75	5.50
XMA	35.56	82.12	46.61
direct integration	PWL = 82.18 dB		-

TABLE 3: SOUND POWER LEVEL FOR SIMULATION SH3

The third test case presented in Figure 6 follows the same principle in terms of methodology. The difference resides in the type of mean flow and acoustic modes imposed in the simulation. In this case the mean flow mimics a duct flow with boundary layers. The prescribed acoustic mode corresponds to $(m, n) = (13,0)$. As the solution is prone to reflections at the inlet, the domain was extended with a buffer zone to reduce reflections.

The difference between XMA and RMA is less pronounced than before (see Figure 7) but there is still a substantial gain with the use of XMA in terms of signal-to-noise ratio as this one rises from 28.42 dB to 40.96 dB (see Table 4).
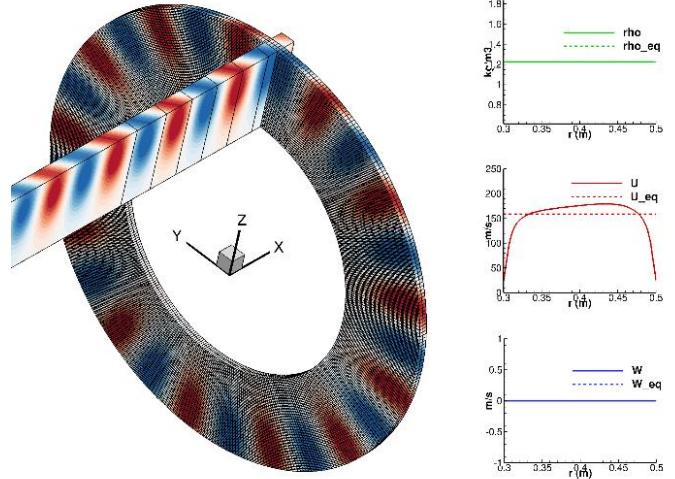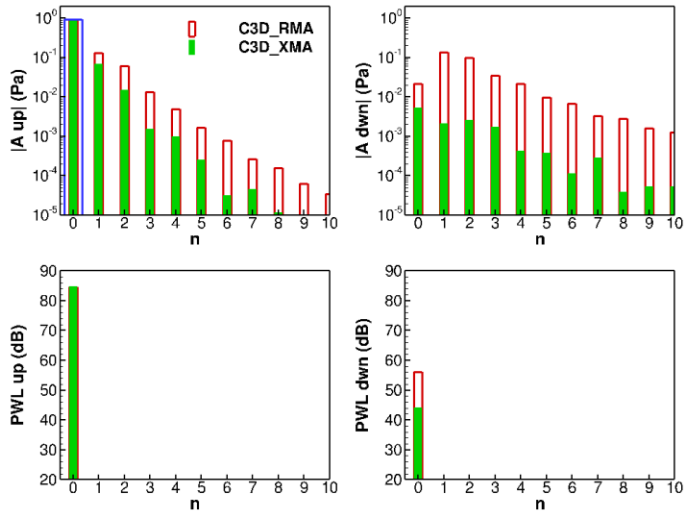

FIGURE 6: GENERIC TEST CASE SH4a WITH BOUNDARY LAYER FLOW

Method	PWL+ (dB)	PWL- (dB)	ΔPWL (dB)
RMA	56.17	84.59	28.42
XMA	43.90	84.86	40.96
direct integration	PWL = 84.92 dB		-

TABLE 4: SOUND POWER LEVEL FOR SIMULATION SH4A

FIGURE 7: ACOUSTIC MODE ANALYSIS OF SIMULATION SH4a; THE TARGETED MODE IS INDICATED IN BLUE

FIGURE 8: (LEFT) FIRST HARMONIC[3] OF THE UNSTEADY PRESSURE FIELD OF THE LOW-SPEED FAN CRAFT, (RIGHT) MEAN FLOW PROFILES

3.2 Application to a low speed axial fan

This section focuses on the application of the mode analysis to more realistic problems. Compared to the generic cases presented before, there are many new aspects coming into play while considering a turbomachine stage simulated by means of the Navier-Stokes equations. Thus, the mean flow is no more axisymmetric and homentropic (usually the entropy changes in the boundary layer), there are regions in the flow where strong vortical disturbances are present, in small arrangement the potential field of the blades can be strong at the positions of analysis, and finally the duct contours may vary. Note that, the pressure saved in the rotating domains is transformed to the absolute frame of reference by means of the following relationship:

$$\omega = \omega_{rot} + m\Omega_{rot}. \tag{13}$$

The first presented application concerns the HB simulation of the low-speed fan CRAFT [32] operated at its aerodynamic design point. The unsteady pressure at the first harmonic extracted just behind the stator is shown in Figure 8. It reveals the presence of small-scale structures due to the wakes as studied by Wohlbrandt et al. [13]. The azimuthal order of the dominant acoustic component is 3 as predicted by the Tyler-Sofrin rule for a rotor—stator stage with 18 rotor blades and 21 stator vanes, respectively. As expected, the flow profiles measured behind the stator do not indicate the presence of a strong swirl. The boundary layers are pronounced but the peak value of the Mach number is below 0.2.

The results obtained by the different extensions of TPP are compared at BPF in Figure 9. The line and colour styles are common to this simulation and the next one discussed in Section 3.3. The direction of propagation is indicated by the colour code: red denotes a propagation in positive, axial direction, i.e. downstream, whereas green denotes a propagation in negative, axial direction, i.e. upstream. Dash lines are used for the results obtained by TPP and solid lines for those by XTPP. Finally, squares represent the results from RMA and circles those from XMA. The black circles highlight the XMA—XTPP combination, which is expected to provide the best results.

Following observations are made:

- The difference between the RMA and XMA results is negligibly small. (Actually, the XMA and RMA curves are on top of each other.) The small Mach number of the flow explains the weak impact of the radial shape of the profiles on the eigenmodes.

- The results from XTPP are more stable (axially less varying) than those from TPP behind the stator. They also exhibit a greater ratio between down- and upstream sound power.

- While the levels obtained by direct integration of the acoustic intensity match well those of the mode analysis in the inlet section, the values are strongly overestimated in the discharge section. This is explained by the presence of strong vorticity disturbances produced by the blades. This makes the use of Eq. (9) not appropriate without filtering.

- The results in the intra-stage indicates that the sound waves emitted in the upstream direction of the stator are rather weakly reflected by the rotor and conversely well transmitted towards the inlet. This illustrates the great use potential of such analysis method.

---

[3] The first harmonic corresponds to BPF in the stator domain.
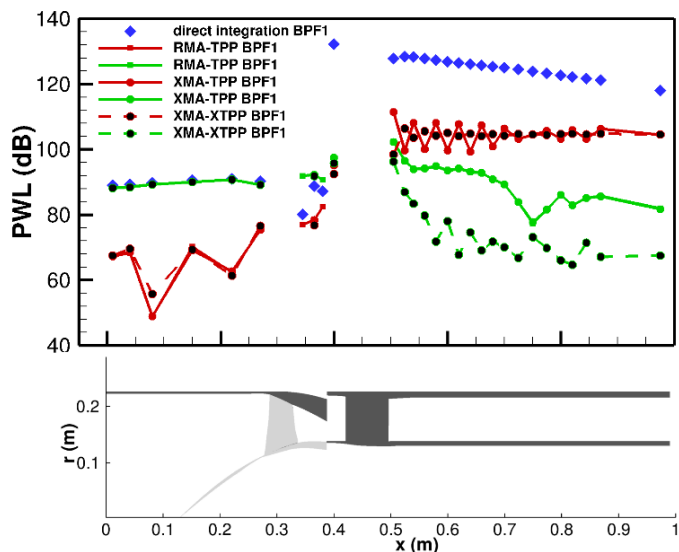
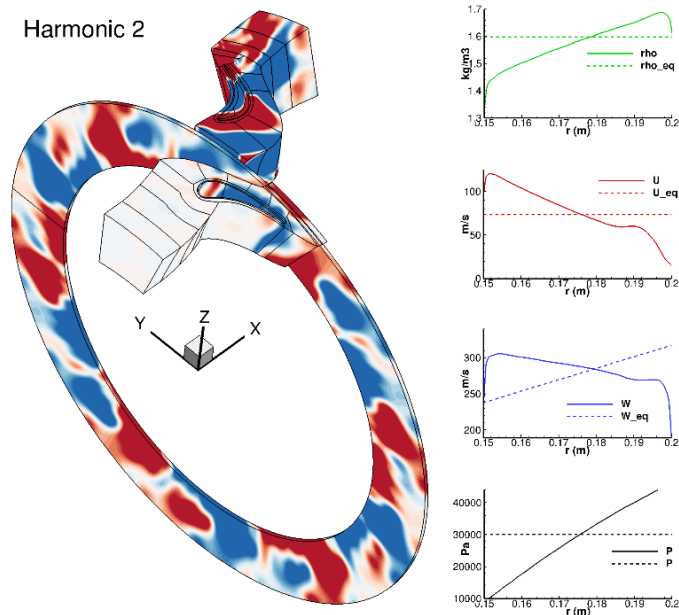**FIGURE 9:** SOUND POWER IN DIFFERENT ZONES OF THE COMPUTATIONAL DOMAIN; LOW-SPEED FAN CRAFT, BPF

3.3 Application to a high-pressure turbine

The second example of application is about the high-pressure, stator—rotor turbine simulation performed and analysed by Holewa et al. [3] in the European project RECORD. An impression of the simulation results at the second harmonic of the pressure is given in Figure 10. In the inlet, the flow is axial, almost uniform, and at low speed ($M_x = 0.1$). On the contrary, the flow in the intra-stage exhibits a very strong swirl reaching up to $M_\theta \approx 0.9$ near the hub. (There is actually a shock on the entry stator vane.) The design of the stator vanes was done using the classical free-vortex laws. Therefore, the rigid body swirl model is particularly inappropriate to approximate the azimuthal mean flow profile. Nevertheless, it enables to account for a mean swirl and as it will be seen in the following results, the integrated results of both solutions, respectively obtained by RMA and XMA, are surprisingly close one another in spite of the strong differences in the assumed mean flow profiles.

The power amplitude calculated at various axial positions of the computational domain is shown in Figure 11. The combination XMA—XTPP (black circles) provides the best results in overall, in particular in the outlet section of the turbine just close to the rotor, where the property of XTPP to better filter the convective perturbations works efficiently.

Particularly challenging for the mode analysis is the zone of the intra-stage, where the swirl is very strong. The highest difference between RMA and XMA is expected to be found there. The results at BPF and 2×BPF are compared for the four method combinations in Figure 12. All values of amplitude are within 4 dB and the difference between RMA and XMA on PWL$_\text{up}$ is around 1 dB, which means that the RMA approach performs quite well. Due to the high Mach number and the high solidity of the stator cascade combined to the high thickness of the profiles, the sound waves emitted by the stator are quasi blocked by the stator. In fact, there is only a difference of about

1 dB between the amplitude of the up- and downstream propagating waves at 2×BPF in the intra-stage. This is consistent with the almost 40 dB difference observed between the waves emitted in the intra-stage and those transmitted in the inlet as indicated by Figure 11. The improvement due to XTPP is not as clear as in the outlet. This deserves further investigations.

FIGURE 10: (LEFT) SECOND HARMONIC OF THE UNSTEADY PRESSURE FIELD OF THE HIGH-PRESSURE TURBINE, (RIGHT) MEAN FLOW PROFILES
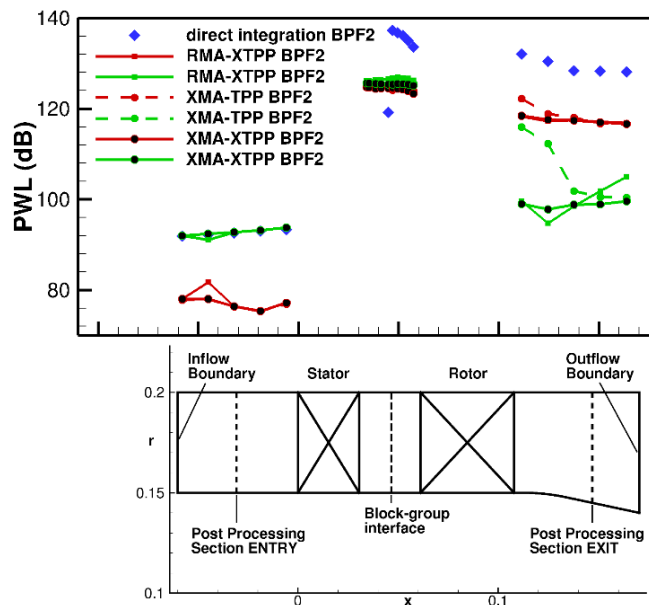
FIGURE 11: SOUND POWER IN DIFFERENT ZONES OF THE COMPUTATIONAL DOMAIN; HIGH-PRESSURE TURBINE, 2×BPF

The results of the mode analysis in Figure 13 indicate that there exist large differences in details between RMA and XMA but the large number of modes counterbalance the error. Luckily,

the cut-off limits are not very different between RMA and XMA. The stronger difference in the eigenvalues k_n for $m = -60$ compared to $m = 6$ (see Figure 14) explains the larger discrepancy for the first cited azimuthal mode.
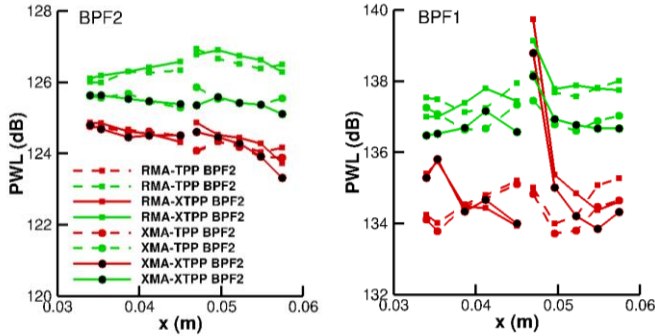

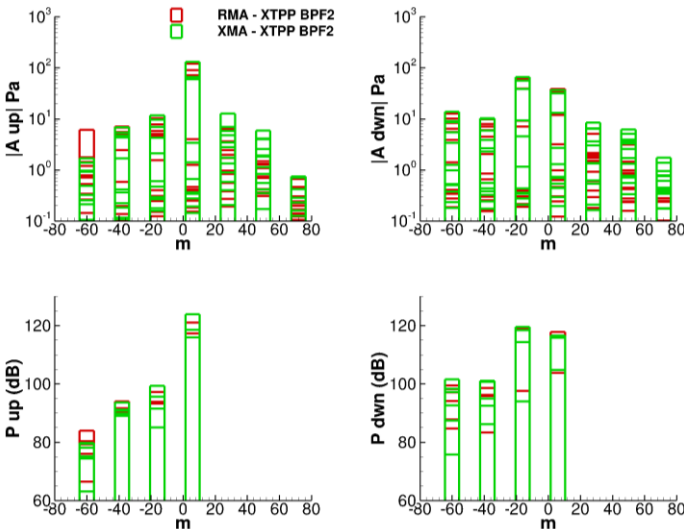**FIGURE 12:** ZOOM ON THE RESULTS OF THE MODE ANALYSIS OBTAINED IN THE INTRA-STAGE

FIGURE 13: ACOUSTIC MODAL DECOMPOSITION IN THE INTRA-STAGE: (TOP) ACOUSTIC PRESSURE AMPLITUDE, (BOTTOM) SOUND POWER, (LEFT) DOWN- (RIGHT) UPSTREAM PROPAGATING WAVES; RADIAL MODES ARE NOT DISTINGUISHED
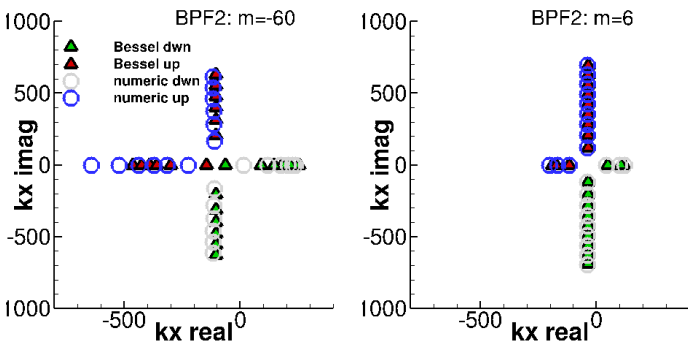

FIGURE 14: AXIAL WAVENUMBER SPECTRA OF TWO AZIMUTHAL MODES; BPF2

4. CONCLUSION

This study has shown that considering the shape of the mean radial flow profiles really improves the detailed results obtained with TPP when the flow exhibits pronounced boundary layers and/or a strong swirl. Particularly critical to the solution is the determination of the cuton—cutoff limit, the prediction of which may vary considerably between the simple and the more elaborate models.

When the mode analysis results have been integrated over the azimuthal spectrum, so that an acoustic level per BPF is determined, the rigid body swirl hypothesis works satisfactorily in the realistic applications studied in this paper. Generally, the error at low speed is small due to the weak impact of the profile shape on the eigenmodes at low Mach number. At high Mach number, two effects oppose each other: on the one hand, Bessel's analytical solutions are imprecise, but on the other hand, the number of cut-on modes is large. The second effect can statistically counterbalance the first, so that the difference in overall level is not as dramatic as one might expect. This should not be taken as a general conclusion but as a likely result.

The investigation downstream of the stages, where strong wake disturbances are present, supports the need for an extension of the triple-plane pressure mode matching technique to include a convective disturbance model. In the narrow space of the small intra-stage, this also seems to be necessary.

REFERENCES

[1] Frey, C., Ashcroft, G., Kersken, H.P. Simulations of Unsteady Blade Row Interactions Using Linear and Non-Linear Frequency Domain Methods, 2015, in Proceedings of ASME Turbo Expo

[2] Kissner, C. A., Guérin, S., Enghardt, L., Siller, H., Pott-Pollenske, S-M., The Challenge of Tonal Fan Noise Prediction for an Aircraft Engine in Flight, 2019, Acta acustica united with Acustica, 105 (1), 17-29, doi: 10.3813/AAA.919284

[3] Holewa, A. Lesnik, S., Ashcroft, G., Guérin, S. CFD-based Investigation of Turbine Tonal Noise Induced by Steady Hot Streaks, International Journal of Turbomachinery, Propulsion and Power, 2017, 2(3)

[4] Jaron, R., Moreau, A., Guérin, S., Enghardt, L., Lengyel, T., Otten, T., Nicke, E. Multidisciplinary design optimization of low-noise and efficient next-generation aeroengine fan. ASME

Journal of Turbomachinery, 2021, 144 (1), 011004. American Society of Mechanical Engineers (ASME). doi: 10.1115/1.4051935. ISSN 0889-504X.

[5] Guérin, S. Farfield Radiation of Induct-Cutoff Pressure Waves, 2017, 23rd AIAA/CEAS Aeroacoustics Conference, Denver, USA.

[6] Ovenden N. and Rienstra S. Mode-matching strategies in slowly varying engine ducts. AIAA J., 2004; 42, 1832–1840.

[7] Giacché D., Xu L. Coupland J, et al. Comparison between postprocessing methods applied to rotor-stator-interaction tone-noise problems. AIAA J 2011; 49: 1214–1229.

[8] Morfey, C. Sound transmission and generation in ducts with flow. J. Sound Vib. 1971, 14, 37–55

[9] Cumpsty, N. A., Horlock, J.H. Averaging nonuniform flow for a purpose. Transaction of the ASME, 2006, 128,120-129.A

[10] Moinier P. and Giles M. B. Eigenmode analysis for turbomachinery applications, J. Prop. Power, 2005, 21(6), 973-978.

[11] Cumpsty, N. A., Horlock, J.H. Averaging nonuniform flow for a purpose. Transaction of the ASME, 2006, 128,120-129.

[12] Weckmüller, C. Hybride Verfahren zur Berechnung der tonalen Schallerzeugung von Turbomaschinen, PhD thesis of the Technical University of Berlin, 2013.

[13] Wohlbrandt, A., Weckmüller, C., Guérin, S. A robust extension to the triple plane pressure mode matching method by filtering of convective perturbations, 2016, International Journal of Aeroacoustics, 15 (1-2), 41-58.

[14] Kousen, K. A., Eigenmodes of Ducted Flows with Radially-Dependent Axial and Swirl Velocity Components, Tech. rep., NASA, 1999, CR-208881

[15] Vilenski G., Rienstra S. W. Acoustic modes in a ducted shear flow, 2005, 11th AIAA/CEAS Aeroacoustics Conference, Monterey (CA), USA, AIAA 2005-3024

[16] Vilenski G. Mode matching in engine ducts with vortical flows, 2006, 12th AIAA/CEAS Aeroacoustics Conference, Boston (MA), USA, AIAA 2006-2584

[17] Morfey, C. L. Acoustic energy in non-uniform flows, J. Sound Vib., 1971, 14(2), 159-170.

[18] Morse, M., Ingard, K. Theoretical acoustics, 1986

[19] Rienstra, S. Sound transmission in slowly varying circular and annular lined ducts with flow ducts Journal of Fluid Mechanics, 1999, 380, 279-296

[20] Pridmore-Brown, D. Sound propagation in a fluid flowing through an attenuating duct Journal of Fluid Mechanics, 1958, 87(4), 396-406

[21] Nayfeh A. H., Kaiser J. E., Telionis D. P. Acoustics of aircraft engine-duct systems, 1975, AIAA J., 13(2), 130-153

[22] Golubev, V. V., Atassi, H. M. Sound propagation in an annular duct with mean potential swirling flow Journal of Sound and Vibration, 1996, 198(5), 601-616

[23] Golubev, V. V., Atassi, H. M. Acoustic-vorticity waves in swirling flows, J. Sound Vib., 1998, 209(2), 203-222

[24] Tam K. W., Auriault, L. The wave modes in ducted swirling flows, J. Fluid Mech., 1998, 371, 1-20

[25] Nijboer R. Eigenvalues and eigenfunctions of ducted swirling-flows, 2001, 7th AIAA/CEAS Aeroacoustics Conference, Maastricht, Netherlands, AIAA 2001-2178

[26] Cooper, A. J., Peake, N. Propagation of unsteady disturbances in a slowly varying duct with mean swirling flow. J. Fluid. Mech., 2001, 445, 207-234

[27] Peake, N., Parry, A. Modern challenges facing turbomachinery aeroacoustics Annu. Rev. Fluid Mech., 2012, 44, 227-248

[28] Kerrebrock, J. L. Small disturbances in turbomachine annuli with swirl, AIAA J., 1977, 15(6), 794-803

[29] M. Roger, H. Arbey: Relation de dispersion des ondes de pression dans un écoulement tournant. Acta Acustica united with Acustica, 1985, 59, 95–101

[30] Weckmüller, C., Hurst J., Guérin S., Enghardt L. Acoustic eigenmodes for ducted sheared mean flow: validation with CAA, 20th AIAA/CEAS Aeroacoustics Conference, Atlanta (GA), USA, AIAA 2014-3117

[31] Mathews J., Peake N., Bianchi S. Asymptotic and numerical Green's function in a lined duct with realistic shear and swirl, 2016, 22nd AIAA/CEAS Aeroacoustics Conference, Lyon, France, AIAA 2016-2922

[32] Tapken, U., Caldas, L., Meyer, R., Behn, M. Klähn, L., Jaron, R., Rudolphi, A. Fan test rig for detailed investigation of noise generation mechanisms due to inflow disturbances, AIAA AVIATION 2021 FORUM, AIAA 2021-2314

[33] Guérin S.., Kissner C., Seeler P., Blázquez R., Carrasco Laraña P., de Laborderie H., Lewis D., Chaitanya P., Polacsek C., Thisse J. ACAT1 Benchmark of RANS-Informed Analytical Methods for Fan Broadband Noise Prediction: Part II—Influence of the Acoustic Models. Acoustics. 2020; 2(3), 617-649. https://doi.org/10.3390/acoustics2030033

[34] Atassi, O. V. 2003, Computing the sound power in non-uniform flow, J. Sound Vib. 266: 75-92.

APPENDIX

The calculation of the sound power assumes that Eq. (8) and (9) can be applied. The amplitude of each mode (m, n) is determined separately and the total power per frequency is obtained by summing the individual contribution:

$$\Pi^{\pm}(\omega) = \sum_{m,n} \Pi_{mn}^{\pm}(\omega). \tag{14}$$

For the Bessel' solution, the modal power amplitude Π_{mn} is given by (see e.g. in Appendix of Ref [33])

$$\Pi_{mn}^{\pm} = \pi R^2 \Re\left\{\frac{\alpha_{mn}}{\rho c \delta_m} C_{mn}^{\pm}\right\} |A_{mn}^{\pm}|^2, \tag{15}$$

where

$$C_{mn}^{\pm} = \frac{(1 - M_x^2)^2}{(1 - \mp \alpha_{mn} M_x)^2}. \tag{16}$$

For the numerically calculated eigensolutions, the power of the azimuthal mode Π_m is obtained by integrating the eigenvectors along the radius. The formalism of Weckmüller et al. [30] is used to express the solution derived from Eq. (8) and (9). The following solution is found for Π_m, where the superscript $(\pm)$ has been dropped for simplicity:

$$\Pi_m = \Re\left\{\sum_{n=0}^{\infty}\sum_{p=0}^{\infty} A_n^* A_p w_{np}\right\}, \tag{17}$$

with

$$w_{np} = \pi e^{i(k_n - k_p)x}\int_{\eta R}^{R}\left[(1 + M_x^2)\hat{p}_n^*\hat{u}_{x,p} + \frac{M_x}{\rho c}\hat{p}_n^*\hat{p}_p \right.$$
$$+ M_x M_\theta \hat{p}_n^*\hat{u}_{\theta,p} + \rho c M_x \hat{u}_{x,n}^*\hat{u}_{x,p}$$
$$\left. + \rho c M_\theta \hat{u}_{x,n}^*\hat{u}_{\theta,p}\right]r\,dr. \tag{18}$$

In this paper, the sound power levels calculated for the numerical eigensolutions discard the cross-terms (such as $p \neq n$), although they are not null since the eigenfunctions are not orthogonal in complex mean flow. As discussed by Atassi [34], the interferences between the radial modes may become significant for solutions in realistic swirling flow. Only at high frequency, they can be neglected and the acoustic power can be assumed to be conserved.